C_3 and NCO($+,0,-$) molecular-ion structure studies by Coulomb explosion

G. Goldring
The Weizmann Institute of Science, Rehovot, Israel,
and Brookhaven National Laboratory, Upton, New York, 11973

Y. Eisen
Soreq Nuclear Research Center, Yavne, Israel

P. Thieberger and H. E. Wegner
Brookhaven National Laboratory, Upton, New York, 11973

A. Filevich
Comisión Nacional de Energía Atómica, Buenos Aires, Argentina
(Received 17 October 1980; revised manuscript received 30 November 1981)

Coulomb-exploded fragments of $C_3^{+,0,-}$, C_4^-, C_5^-, C_6^-, and $NCO^{+,0,-}$, following stripping of high-energy molecular ions in a thin carbon foil, were recorded, first in plastic sheet detectors, and in later experiments with a new image-intensifying and digitizing system. All of the ions studied in detail, C_3 and $NCO^{+,0,-}$, appear to be formed in states of high bending excitations perhaps close to the dissociation limit. The intranuclear separations for the C_3 species were found to be similar to that of normal neutral C_3, 2.5(1) Å; and for the NCO species, rather small, 2.0(1) Å.

I. INTRODUCTION

The experiments described here are an attempt to gain structure information on a number of complex molecular ions by observing the Coulomb explosion of the molecular fragments produced when a beam of high velocity molecular ions passes through a foil and the molecules are stripped of electrons and break up in the process. The method in general is well documented and has been applied, for example, to the study[1] of H_3^+. A comprehensive review is given by Gemmell *et al.*[2] The present work is concerned in particular with positive, neutral, and negative forms of NCO, $NCO^{+,0,-}$ and also of C_3, $C_3^{+,0,-}$. The C_3^- ion is a member of a family of molecular ions, C_n^- with n ranging from 2 to at least 12, which are copiously produced in sputter ion sources. Very little is known about the structure of these ions or the excitation regime of ions produced by the sputtering process. Other measurements reported here concern the Coulomb explosion of C_4^-, C_5^-, and C_6^- ions and also the breakup of 4-MeV NCO^- ions by gas collisions into the diatomic species NC^+, CO^+, and NO^+.

Two new types of detectors for such measurements were employed in this experiment: the first was a polycarbonate sheet treated, after exposure to the incident ions, by electrochemical etching.[3] It was shown during the present experiments that these detectors are sensitive to C, N, and O ions at energies well below 1 MeV and that Coulomb-explosion images were clear and generally free of obscuring background. The second detector was an image-intensifier detection system[4] which allowed acquisition of data of high quality and good statistics. Even though this new technique provides data of high quality and good statistics, the extent of information gained on molecular-structure details is rather limited. All the ionic species studied appear to be in geometrically similar configurations. They can be interpreted as resulting from states of high bending excitation close to the dissociation limit. In this interpretation, the details of the molecular structure are effectively masked by the excitation pattern of the bending vibrational modes. Definite information was derived on intranuclear separations: in both C_3 and NCO the separations were found to be very similar for the different charge states. For the C_3 species the intranuclear separation was found to be 2.5(1) Å, close to the spectroscopically measured separation of neutral C_3, and for NCO the overall length was found to be rather small, 2.0(1) Å.

II. EXPERIMENTAL PROCEDURE

The injector MP tandem, which is the first accelerator of the Brookhaven National Laboratory three-stage Van de Graaff facility, is equipped with a sputter ion source[5] inside the high-voltage terminal that provides negative ions for three-stage acceleration. This source produces carbon-molecular ions ranging from C_2^- to C_{12}^- as illustrated in Fig. 1 which shows the mass spectrum from the ion source when it is being operated with a carbon cone. The data shown were taken with an external source similar to that used in the high-voltage terminal and the negative carbon-molecular ions were identified by accelerating them through the tandem accelerator and measuring the magnetic rigidity of the resulting positive carbon ions.

In this experiment, the terminal sputter ion source was used to provide accelerated C_3^-, C_4^-, C_5^-, and C_6^- molecular ions from a carbon cone and NCO^- molecular ions from a potassium cyanate (KOCN) cone. These ions were then magnetically analyzed for proper mass identification followed by "supercollimation"[6] as shown in Fig. 2. The two adjustable apertures are followed by a permanent magnet and adjustable steering magnet that provide a 5° deflection of the negative ions with the same mass product as the 90° analyzing magnet. This final deflection removes all of the negative ions that have been slit or gas scattered because the scattered ions are either neutral or positive, and consequently, removed from the beam. Horizontal and vertical cleanup slits adjusted to be close to but not touching the supercollimated beam ensure an extremely clean microbeam with sharp edges of a size varying from 0.05 to 1.0 mm diameter, depending on the selected aperture settings. After the beam is steered through the various apertures it is decreased in intensity to a few thousand ions per second as monitored by a solid-state detector. Final steering adjustments are then made to ensure that the beam is going through the center of a 1-μg/cm^2 carbon stripping foil which is mounted on a 3-mm-diam foil holder.

Once the final steering correction has been made, the intensity is decreased to approximately 2−5 counts per second by decreasing the aperture sizes

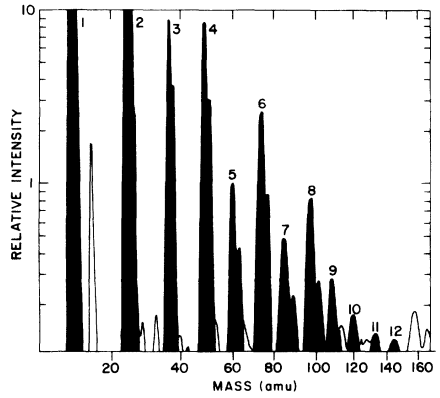

FIG. 1. Mass spectrum of negative ions produced by a cesium sputter ion source operated with a carbon cone. Numbers indicate the molecular mass of multiple carbon ions which were positively identified.

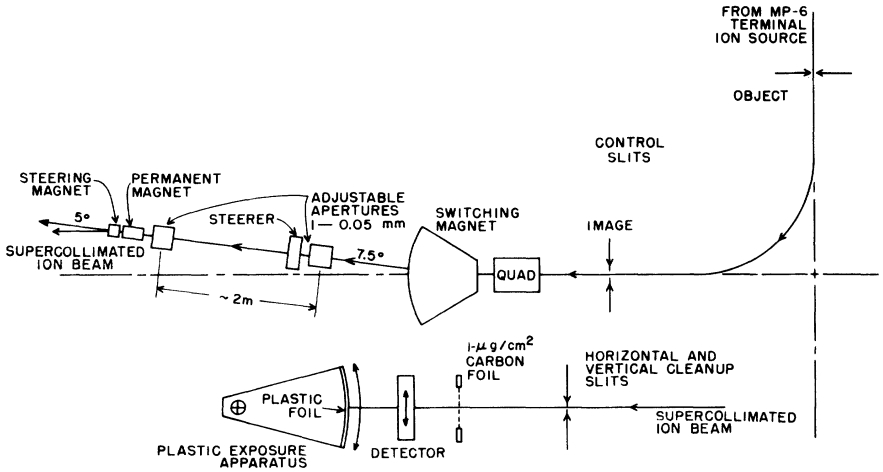

FIG. 2. Schematic layout of the experimental arrangement for supercollimation of the accelerated negative molecular ions and the mechanical arrangement for exposing polycarbonate plastic sheets to the Coulomb-exploded ions. (See text for details.)

further and closing down the object slit of the 90° analyzing magnet with all quadrupoles in the beam transport turned off. In addition to attenuating the beam, this procedure also enhances its optical quality. $NCO^{+,0}$ and $C_3^{+,0}$ ions were produced by gas exchange of the accelerated NCO^- and C_3^- ions either in the gas-stripper canal of the tandem accelerator or in the residual gas in the beam-transport system after the switching magnet (vacuum 10^{-6} to 10^{-7} torr).

The Coulomb-exploded ions were first detected in polycarbonate plastic sheets[3] of $0.037\times3\times5$ cm^3 and mounted as shown schematically in Fig. 2. The target to detector distance varied between 2.5 and 7 cm. The holder was rotated back and forth and raised and lowered manually. It was stepped vertically 2 mm before each rotary scan which would have resulted in a uniform exposure of 10–20 events per cm^2 if the beam current had been absolutely stable. Unfortunately, beam-current fluctuations caused frequent event clustering; however, many single events were observed. After exposure, the plates were developed by an electrochemical etching technique[3] and a typical exposed plate is shown in Fig. 3. A number of spots in each exposure were artifacts of various kinds and could be eliminated by observation through a microscope with a magnification of 100×. A small number of background spots persisted even at high magnification and could conceivably give rise to artifact "molecules" or correlated events. It was conservatively estimated that the fraction of such unreal events is at most 0.03.

Figures 4, 5, and 6 show examples of isolated three, four, and five carbon events corresponding, respectively, to C_3^-, C_4^-, and C_5^- ions of 4.67, 3.50, and 2.80 MeV. The energy of the carbon atoms in the C_5^- exposure is 560 keV; the lowest energy so far recorded by this method. The detection efficiency appears to be close to 100% even at this low energy. The jagged-edge spots are characteristic of heavy-ion tracks with this etching technique. A few events show all three atoms of the C_3^- molecule closely spaced as shown in the lower right-hand examples of Fig. 4. These events could be due to molecular dissociation by collisions with residual gas molecules in the transport system followed by subsequent stripping in the carbon foil with very little or no Coulomb-explosion effect. Such events illustrate the excellent spatial resolution of this detection method which is smaller than the diameter of the spots.

Altogether, less than 100 events were identified unambiguously and recorded with this etching method for each species. The triatomic systems appeared considerably more "triangular" than was expected for exploding rodlike structures, but the poor

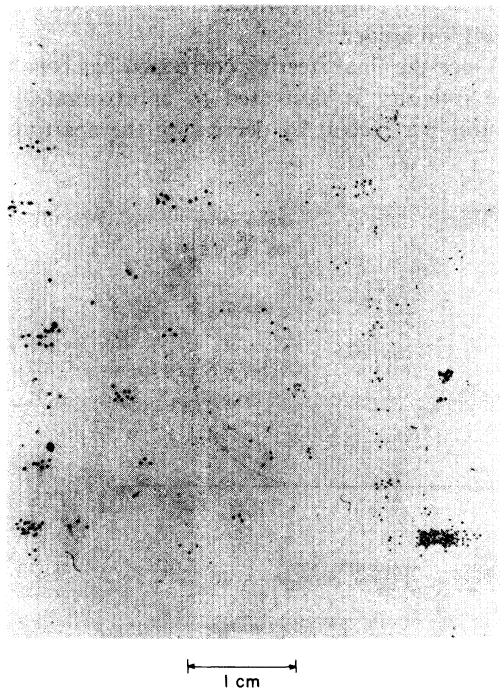

FIG. 3. Partially magnified electrochemically etched polycarbonate foil after exposure to stripped 4.67-MeV C_3^- ions.

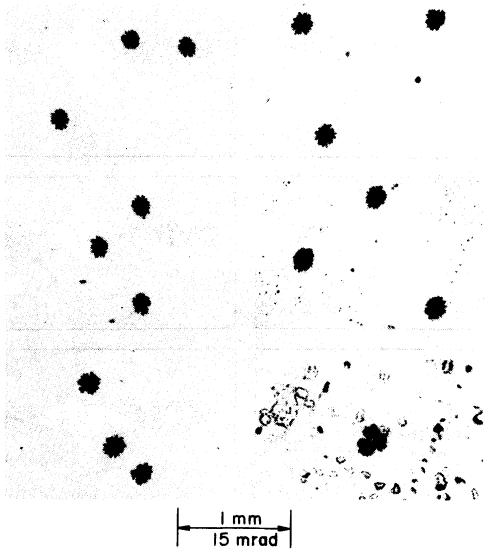

FIG. 4. Further magnification of selected C_3^- molecular explosion events at 4.67-MeV molecular-ion energy.

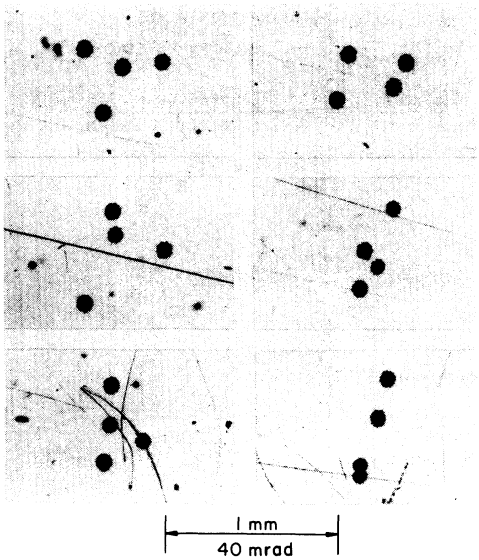

FIG. 5. Selected C_4^- molecular explosion events at 3.50-MeV molecular-ion energy.

statistical quality of the samples precluded any definite conclusions. A new electronic system of detection based on an image intensifier was therefore developed, and it was employed for obtaining the data discussed subsequently in this paper.

The experimental requirement of detecting simultaneous multiple low-energy heavy ions from the Coulomb explosion of accelerated molecules has led to a detector[4] consisting of a thin monolayer phosphor coating with particle size approximately 1 μ

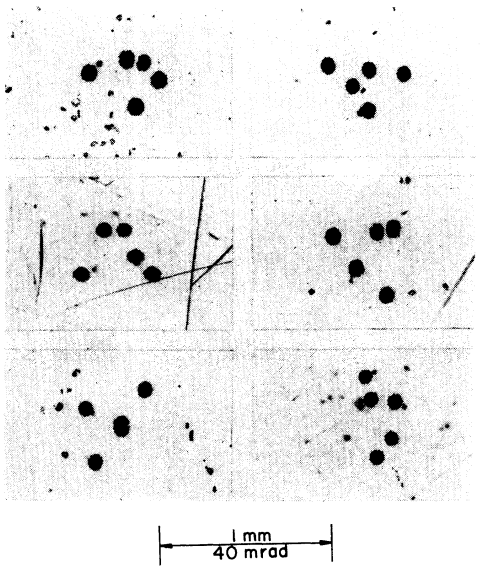

FIG. 6. Selected C_5^- molecular explosion events at 2.80-MeV molecular-ion energy.

applied uniformly on the input fiber-optic plate of a commercially available image intensifier. The phosphor particles scintillate when struck by atomic ions formed by the breakup of molecular ions when passed through a thin carbon foil. The faint scintillations are amplified by the image intensifier whose output is viewed by a television camera. The television image is then digitized and the pixels containing useful information are stored for later analysis.

The experimental arrangement for the imaging of Coulomb-explosion events is shown schematically in Fig. 7. A 60-cm flight path provides an adequate distance so that the spreading particles are conveniently separated when they impinge on the scintillation screen. An alpha-particle source and silicon detector can be inserted into the beam line for test purposes. A calibration plate containing a number of tiny apertures of known spacing can also be inserted between the stripping foil and the scintillation screen in order to provide an absolute calibration of the angular spread of the Coulomb-exploded molecular-ion components. A television camera views the 25-mm-diameter output fiber-optics plate with magnification arranged to fill most of the vertical dimension of a conventional television monitor. A small photomultiplier tube adjacent to, and off axis from, the camera lens is also exposed to the amplified scintillation light and provides fast trigger signals that are used by the logic of the television digitization system. A detailed description of this detection system is given in Ref. 4.

A commercially available television digitizing system based on a Z80 microprocessor and provided with a 64-K byte memory and two 8-in floppy disks for system programs and data storage is used to digitize the scintillation light images provided by the television camera. The system digitizes the camera video signal continuously and with the aid of the photomultiplier trigger signals, selects and stores Coulomb-explosion events of interest. When the buffer store in memory is full, the data are transferred onto a floppy disk which can later be read into a file of an XDS Sigma 7 computer for further analysis. The software is conveniently arranged to allow live monitoring of the events that are being stored as well as step-by-step event control.

The computer program used to analyze the digitized data checks each event to insure that it consists of the correct number of scintillations of appropriate size and intensity and rejects all others. The centroid of the fragments is evaluated for each

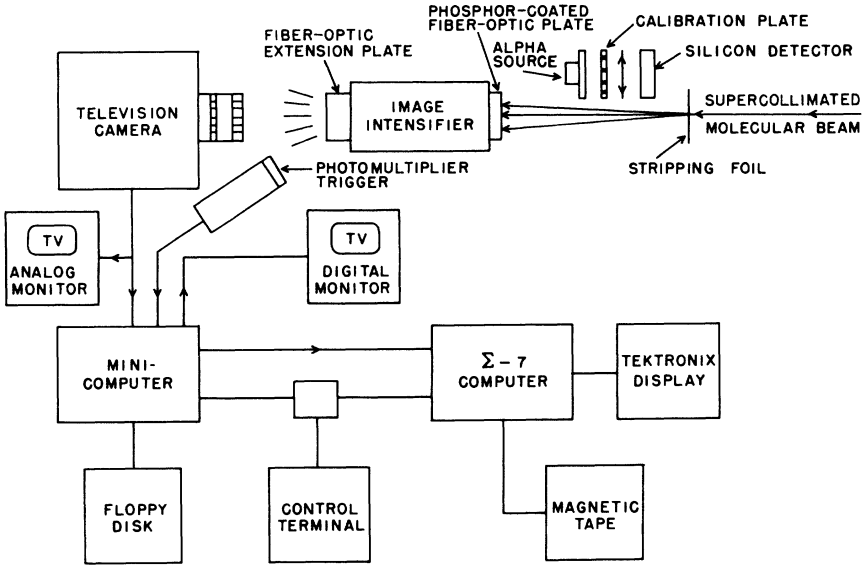

FIG. 7. Schematic diagram of image-intensifier detector system and television readout and digitizing system (see text).

event and the few events with centroids far removed from the beam axis are rejected. These are probably spurious coincident events caused by fragment ions that have been produced by breakup of the original molecules in the residual gas in the vacuum line before passing through the stripping foil. The fraction of rejected events was approximately one half, mainly due to the wrong number of scintillations.

Typical Coulomb-explosion events for 4.67-MeV C_3^- molecules are shown in Fig. 8 which are plots from a Tektronix display of the digitized data. The scales correspond to the actual distance on the scintillation screen in millimeters and the corresponding angular spread in milliradians. The system can detect carbon ions at least down to 300 keV in energy. Similarly, selected Coulomb-explosion events for 3.50-MeV C_4^-, 2.80-MeV C_5^-, and 2.33-MeV C_6^- molecules are shown in Fig. 9. Several hundred of those more complex molecular explosions have been observed and recorded.

III. EXPERIMENTAL RESULTS

A. Breakup of NCO^- ions into diatomic species

In addition to the Coulomb-explosion method of totally breaking up a fast molecule in a thin foil, with subsequent study of the fragments, partial breakup measurements can be made that give some insight to the possible structure of the molecule. The gas stripper canal inside the high-voltage terminal of the tandem accelerator was used to provide a partial breakup of the triatomic molecule to diatomic and monoatomic fragments. The initial molecular ion produced in the ion source is an NCO^- ion. It is accelerated to 2 MeV at the high-voltage terminal where it interacts with a low-density gas inside of the stripper canal and partially

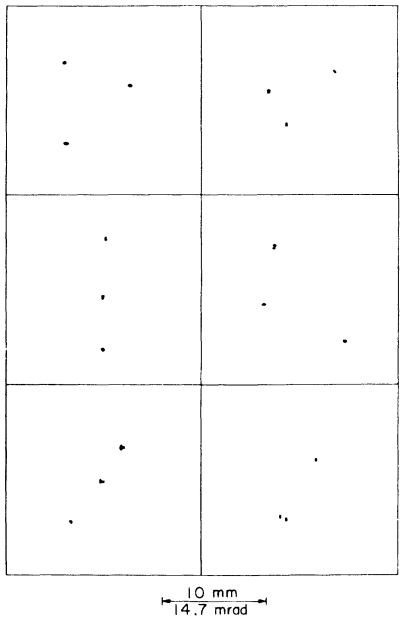

FIG. 8. Typical C_3^- Coulomb-explosion data as plotted from a Tektronix display.

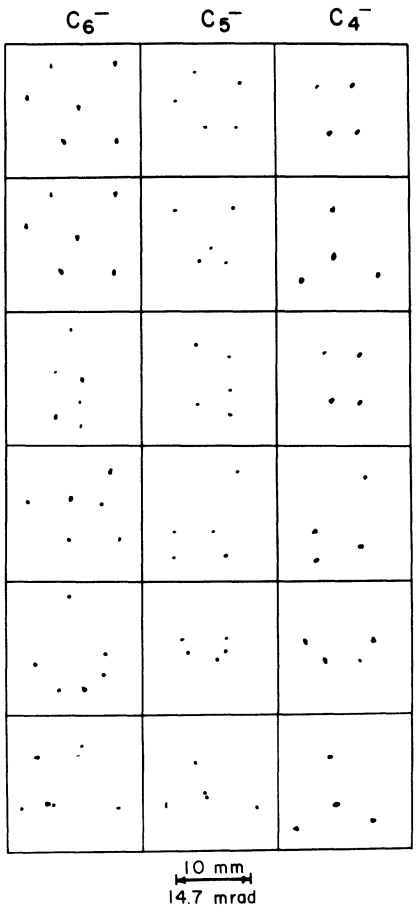

FIG. 9. Typical $C_{4,5,6}^-$ Coulomb-explosion data as plotted from a Tektronix display.

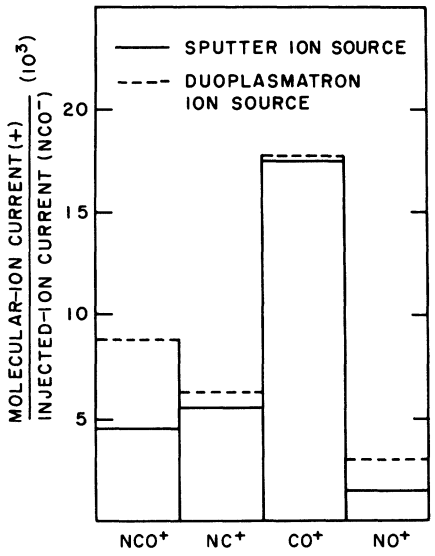

FIG. 10. Comparison of charge exchange and diatomic breakup of 4-MeV NCO^- ions produced by two different ion sources.

breaks up, forming a mixture of NCO^+, NC^+, CO^+, NO^+, N^+, C^+, and O^+ ions, as well as other unobserved charge states. The efficiency for producing the positive diatomic and triatomic molecules is only 1−2%, however, the relative intensities of the diatomic species allow some insight to the possible structure of the negative ion initially accelerated. If the NCO^- ion is a linear structure, then when it is broken into diatomic fragments, NC^+ and CO^+ ions, but no NO^+ ions, would be expected. Similarly, if the structural sequence were CNO^- the breakup products CN^+, NO^+, and no CO^+ would be expected. Measurements of this kind were undertaken with NCO^- from two ion sources: a sputtering source and a duoplasmatron source, and the results are shown in Fig. 10. It appears that the two sources produce negative ions of very similar structure as indicated by the respective breakup pattern. There is in both a small fraction of NO^+ ions which may, perhaps, indicate a fraction of NCO^- ions in either a CNO or a triangular form.

B. Coulomb-explosion results

The Coulomb-explosion events of triatomic molecules require three parameters for their complete characterization, e.g., the three sides of the triangle formed by the three projections of the momenta of the three atomic ions onto the plane perpendicular to the beam. For the sake of simplicity of display and analysis we have reduced the number of parameters to two, as shown in Fig. 11: the largest side l, and the ratio $R = d/l$ where d is the altitude to the side l, integrating over the asymmetry δ/l, considered to be the least significant parameter for structure characterization.

Two-dimensional sorts versus d/l and l for the Coulomb explosion of positive, negative, and neutral 4-MeV NCO molecules are shown in Fig. 12(a) and, similarly, for 4.67-MeV C_3 molecules in Fig. 12(b).

It is apparent from the figures that the distributions for the three different charge states are very similar. The shapes of the NCO distributions are also similar to the C_3 distributions, however, the NCO distributions have a mean l value approximately 2 mrad larger than that of C_3. All of the data extend out to the d/l limit of 0.866, corresponding to an equilateral triangle shape.

A more detailed comparison of the two-dimen-

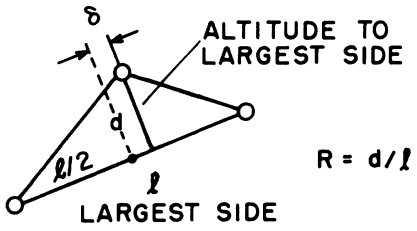

FIG. 11. Triangle parameters for a triatomic Coulomb-explosion event.

sional plots of the different molecules can be made by projecting all of the data on either the l or the d/l axis. The l distributions relate most closely to the size of the molecular ion, whereas the d/l distributions are most intimately associated with the molecular shape. Projections of the data shown in Figs. 12(a) and 12(b) onto the l axis are shown in Figs. 13(a) and 13(b), respectively. These projections, which are area normalized for comparison, show again and more clearly, that the mean l of the NCO and C_3 distributions differ by about 2 mrad and that the relative width of the NCO distribution is also somewhat larger than that of the C_3 distribution. The l distributions of $NCO^{+,0,-}$ ions are very similar; however, C_3^- appears to have a mean l larger than C_3^0 and C_3^+ by 0.2 or 0.3 mrad. The solid-line curves are theoretical fits to the data and will be discussed later.

Projections onto the d/l axis of the two sets of data of Figs. 12(a) and 12(b) are compared in Figs. 14(a) and 14(b). These projections show that there is little difference in the d/l distribution between the three charge states of either of the triatomic systems and there is also no significant difference between the two different triatomic systems. It is interesting to note that the NCO^0 distribution shows a trend for a modest peaking at small d/l ratios compared to $NCO^{+,-}$ and this trend is also

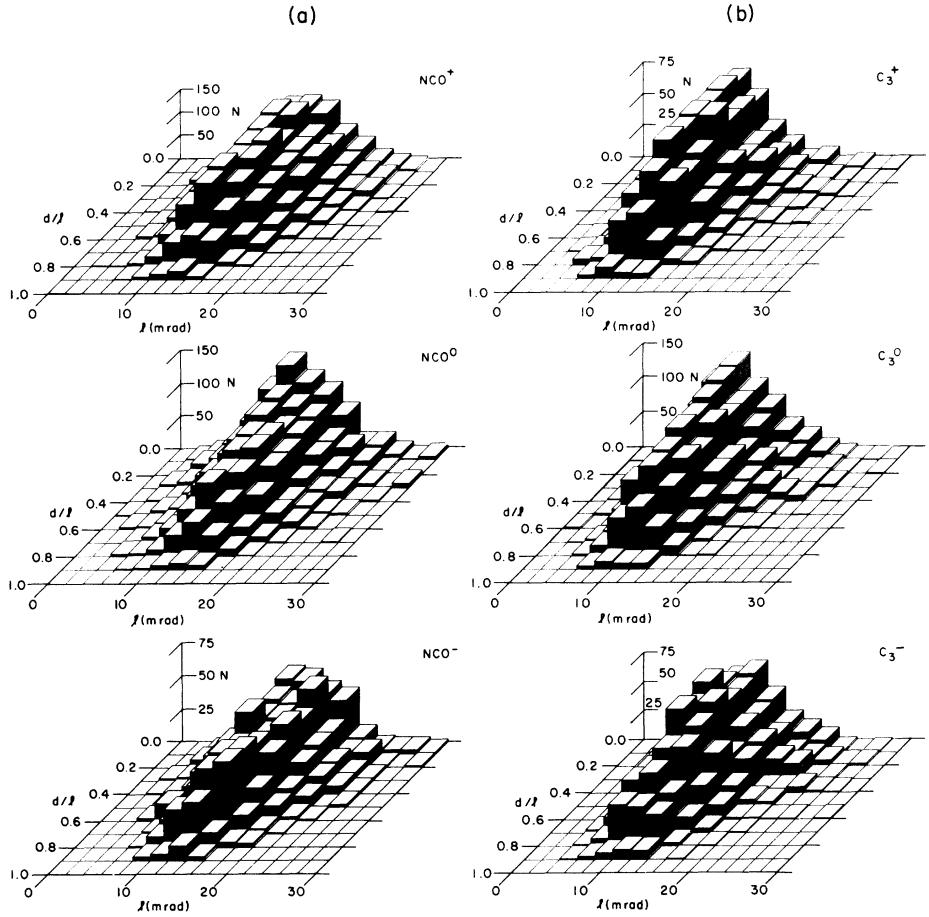

FIG. 12. (a) Summary of $NCO^{+,0,-}$ molecular explosion events plotted as a function of l and d/l. (b) Summary of $C_3^{+,0,-}$ molecular explosion events plotted as a function of l and d/l.

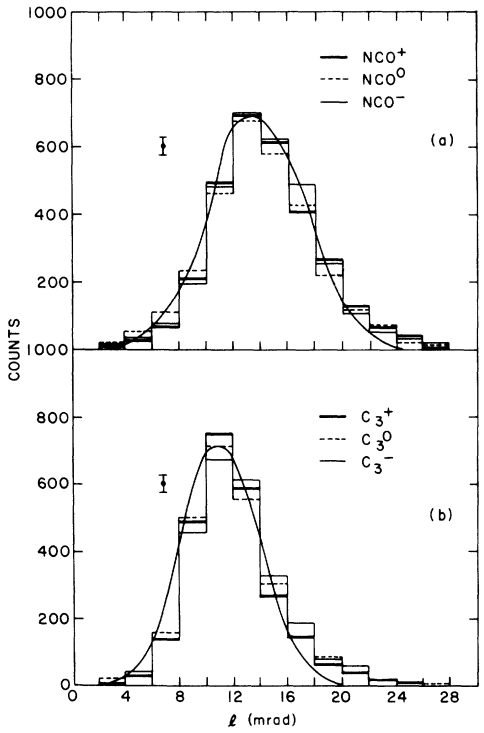

FIG. 13. Projections onto the l axis of the two-dimensional distributions shown in Figs. 12(a) and 12(b). Isolated points indicate the statistical accuracy of the bars on the histogram. Curves through the histogram correspond to theoretical fits (see text).

noticeable in the isometric display of Fig. 12(a).

For the sake of comparison with model calculations the data have been reduced in yet one more way: the shape distributions—the d/l projections—have been sorted according to the magnitude of l and only 40% of the data pertaining to the largest l (the largest "largest sides") have been retained. This selection has the following advantages: large (projected) triangles are less sensitive to the perturbations caused by multiple scattering and such triangles largely exclude configurations in which two fragment ions are aligned along the beam direction (perpendicular to the projection plane), considerably reducing the significance of wake effects.

A comparison has also been made of NCO Coulomb explosions from molecules produced in both the sputter and duoplasmatron ion source. The l and 40% d/l projections of the respective NCO^+ ions are shown in Figs. 15(a) and 15(b). The distributions for the two sources are obviously very similar, in accord with the similarity in the breakup product distribution discussed earlier (cf. Fig. 10).

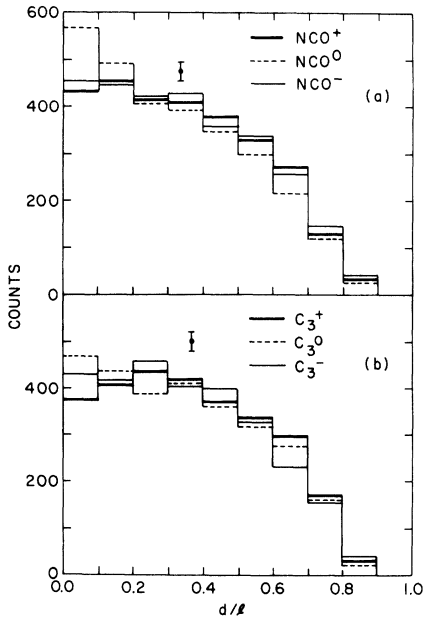

FIG. 14. Projections onto the d/l axis of the two-dimensional distribution shown in Figs. 12(a) and 12(b). Isolated points indicate the statistical accuracy of the bars on the histogram.

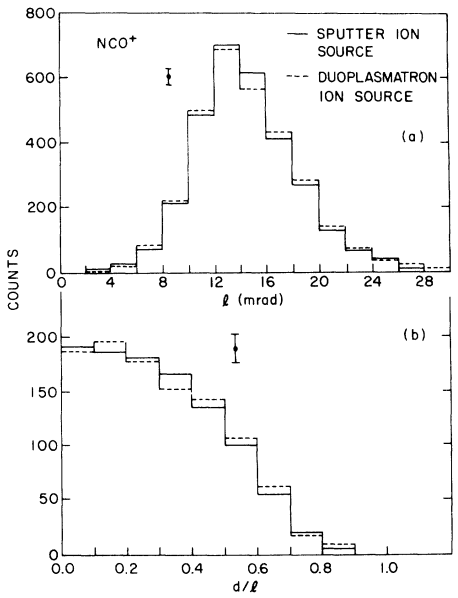

FIG. 15. (a) Comparison of the l distributions corresponding to the Coulomb explosion of NCO^+ ions produced by a sputter and a duoplasmatron ion source. (b) Comparisons of the d/l distributions as in (a) but corresponding only to the 40% fraction of the largest triangles of the distribution. Isolated points indicate the statistical accuracy of the bars on the histogram.

The data presented here were compared with model calculations based on assumed molecular shapes and excitations. Charge-state distributions were measured for N, C, and O ions at energies corresponding to their respective energies as atomic components of the molecules used in these measurements. Owing to a recently discovered cluster effect, the charge-state distributions for closely correlated ions are different from those for single ions as measured here[7]; consequently, appropriate small corrections, based on the data of Ref. 7, were applied to the measured charge distribution in the model calculation.

As an introduction to the model calculations, a brief survey of the factors governing the molecular shape and the evolution of the system from its initial stage to the final projection recorded in the detector will be presented.

IV. PROCESSES THAT SHAPE THE MOLECULAR BREAK UP

A. Molecular excitation and motion

The excitation regime of the molecular ions is largely determined by processes occurring inside the ion source. Changes in excitation during the transport to the stripper foil are governed by the molecular and instrumental time constants: the mean lives of electronic and vibrational excitations are of the order of nanoseconds and milliseconds, respectively, while the transport time is several microseconds. The electronic excitations therefore largely decay even before the ions exit from the ion source whereas the vibrational excitations remain in the pattern established in the source. As the ions reach the carbon foil, they are stripped in a time of $\sim 10^{-16}$ sec. Since the vibrational periods are of the order of 10^{-13} sec, the stripping essentially constitutes a snapshot of the vibrational wave function. The Coulomb explosion and its correlated orientation of the molecular fragments then evolve from that moment. Molecular rotations have a relatively small effect on the Coulomb explosion and the molecular orientation upon entering the foil is completely random with respect to any spatial orientation.

Most of the experiments described here involved a sputter ion source, and no prior information was available on the prevailing vibrational temperatures under these circumstances of ion production. In part of these experiments both NCO^- and C_3^- were stripped to NCO^+, C_3^+ and NCO^0, C_3^0. This process, presumably, will not affect the molecular excitation if the two ions are well matched in their structure. If, however, their shapes are different, it is expected that the excitation pattern will change; the predominant vibrational states of the positive and neutral ions will presumably be those that have the largest overlap with the prevalent NCO^- and C_3^- states.

B. Dynamics and kinematics of the Coulomb explosion

The Coulomb explosion proceeds from initial positions distributed according to

$$\sum_{n_1 n_2 n_3} a_{n_1 n_2 n_3} \left| \psi_{n_1}(x_1)\psi_{n_2}(x_2)\psi_{n_3}(x_3) \right|^2 ,$$

where n_i are the quantum numbers, x_i the coordinates, and $\psi_{n_i}(x_i)$ the wave functions of the normal vibrational modes. The initial stage of the explosion occurs inside the foil, with the fragments acquiring about $\frac{1}{4}$ of their final kinetic energy. The fragments of any atomic species have a common mean charge at this stage. As the fragments emerge from the foil they assume definite fixed charges which determine the final phase of the Coulomb explosion. For the sake of simplicity, we ignored the first phase in our calculations (assuming, in effect, an infinitely thin stripper foil). We expect the errors due to this approximation to be negligible in the present case.

A complete analysis of the Coulomb-explosion events would imply a rigorous inversion of the interaction—a unique assignment of an initial nuclear configuration to every observed event. This is a difficult procedure because of the large geometrical distortions that are caused by the Coulomb-explosion process when fragments of similar masses are involved. The distortions inherent in such a transformation are shown in Fig. 16 which illustrates the explosion of three ions of equal mass and charge, forming an isosceles triangle. The final configuration is also an isosceles triangle and Fig. 16 shows the opening angle α_f of the final configuration as a function of the initial angle α_i. It is evident that there is a wide range of initial angles that transform into nearly equal final angles ($\sim 60°$) and the inverse transformation is not unique: to every final angle there correspond, in general, two initial angles. [Strictly speaking, the entire mechanical process is uniquely defined and uniquely transformed; however, the two solu-

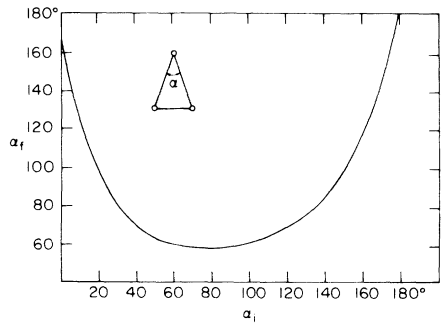

FIG. 16. Initial and final apex angles of isosceles triangles of three particles of equal mass and charge experiencing a Coulomb explosion.

tions corresponding to one α_f between the velocity vectors (and assuming the potential energy to be equal for both) differ only by a minute amount in the coordinates at any given time.] The problem is further complicated by the nonisotropic interaction between the ions while inside the stripping foil.[8] This interaction affects mostly ions that are approximately lined up along the direction of the molecular-velocity vector. An additional uncertainty is introduced by multiple scattering of the fragment ions in the foil. Nevertheless, it will be shown presently that significant information of molecular structure can be obtained in experiments of this kind.

V. MODEL CALCULATIONS

The neutral NCO and C_3 molecules were chosen as models for the various NCO and C_3 species. These are collinear structures with NCO in the N−C−O configuration and their vibrational motion has the three normal modes indicated in Fig. 17. The normal frequencies and the internuclear separations are given in Table I.[9] The lowest frequencies are in the bending mode and C_3, in particular, is a rather "floppy" rod.

The bending mode appreciably affects the shape of the molecules (the d/l ratio). The other two modes would affect mainly the overall size (the l parameter) but their average influence is small.

In the bending mode the system is characterized by the angle θ indicated in Fig. 17. The probability $P(\theta)$ of finding the system at angle θ is given by the square of the wave function $\psi_n^2(\theta)$ which in the harmonic limit is

$$P_n(\theta)=\psi_n^2(\theta)\simeq H_n^2(\alpha,\theta)e^{-\alpha^2\theta^2}$$

with

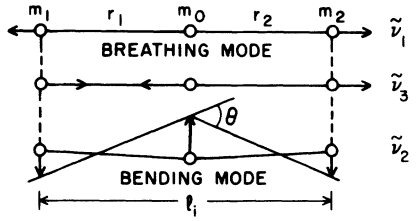

FIG. 17. Bending and breathing modes of vibration for a rodlike triatomic molecule.

$$\alpha^2=\frac{\mu\pi c\tilde{\nu}_2 l_i^2}{2\hbar}$$

and

$$\mu=\frac{m_1m_0m_2}{4m_1m_2+m_0(m_1+m_2)}\ ,$$

where H_n is the Hermitian polynomial of nth order, $\tilde{\nu}_2$ is the bending frequency in cm^{-1}, $l_i=r_1+r_2$ is the maximum separation between the outermost atomic constituents of the molecule, and m_0, m_1, and m_2 are their respective masses. The mean square angle is given by

$$\langle\theta^2\rangle_n=\frac{1}{\alpha^2}(n+\tfrac{1}{2})\ .$$

For large n ($n\geq 6$), the classical approximation is used:

$$P_n(\theta)\begin{cases}\sim\dfrac{1}{(a_n^2-\theta^2)^{1/2}}, & \theta^2<a_n^2\\ =0, & \theta^2>a_n^2\end{cases}$$

with $a_n^2=2\langle\theta^2\rangle_n$.

It was established that for $n=6$ the difference between the d/l distribution computed classically and quantum mechanically was less than the experimental sensitivity.

Multiple scattering occurs concurrently with the Coulomb explosion inside the foil and can, under certain circumstances, considerably affect the breakup pattern.[10] An accurate representation of the multiple scattering was not made in these calculations but simplified approximations were used and are believed to be adequate. The effect of multiple scattering on the d/l distribution for large l has been computed for two extreme conditions: the scattering occurring wholly before or after the Coulomb explosion. The two respective distribution functions were found to be rather similar and the modifications entailed by both of them are rather marginal. The mean scattering angle (half width at half maximum) was taken in these calculations to

TABLE I. Molecular constants for NCO and C_3.

	$l_i=d_j+d_2$ (Å)	$\tilde{\nu}_1$ breathing (cm^{-1})	$\langle(x-l_i)^2\rangle_0^{1/2}$ (Å)	$\tilde{\nu}_2$ bending (cm^{-1})	$\langle\theta^2\rangle_0^{1/2}$ (rad)	$\tilde{\nu}_3$ (cm^{-1})
NCO	〈2.37 2.0(1)[a]	2338	0.061	681	0.12	1284
C_3	2.56 2.5(1)[a]	1230	0.094	63	0.32	2040

[a]Present measurement.

be 1.0 mrad. This value was derived with minor extrapolations from a measurement of the scattering of the center of gravity of the breakup products of each of the different molecules studied.

VI. RESULTS AND DISCUSSION

The comparison of the calculated distributions with the data was carried out as a two-parameter fit for the equilibrium separation $l_i=r_1+r_2$ and the bending vibrational amplitude. Calculated d/l distributions at large l based on the bending frequency of NCO are shown in Fig. 18(a) and compared with the measured distribution for $NCO^{+,0,-}$ ions. A good fit except for small d/l values is obtained for $n=7$. A distribution of excited states centered at about $n=7$ could evidently be just as adequate. A similar comparison is made in Fig. 18(b) for the measured distribution of $C_3^{+,0,-}$ ions. Here the best fit is obtained for $n\sim 2$ which is much lower than the value for NCO because of the low bending frequency. Again, the persistent peaking at small d/l values is observed in the calculated distribution for small d/l values. These observations can be summarized in the following way: the data for all the species investigated can be fitted, with the exception of the small d/l region, with oscillator states that have classical amplitudes of approximately 40°.

The peak at small d/l in the calculated distributions is clearly associated with molecules close to a straight rod configuration ($\theta\simeq 0$). Such predicted needle-shape molecules must be almost completely absent in order to account for the experimental data. In fact, from a purely geometrical approach, the data can be reproduced by assuming a superposition of initial triangle structures with external angles θ, ranging from $\sim 10°$ to $\sim 40°$. These are remarkably high bending amplitudes and they may also explain the fraction of NO^+ observed in the breakup of NCO^-.

The molecules all appear to be in states of high bending vibrational excitation characterized more

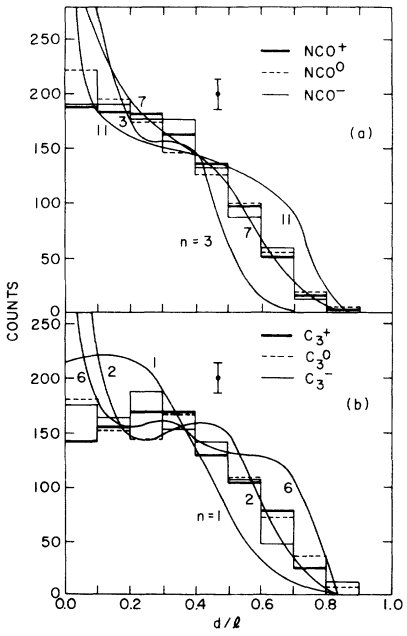

FIG. 18. (a) Projections onto the l axis of the two-dimensional distributions shown in Fig. 12(a) corresponding to the 40% fraction of the largest l triangles of the distribution. (b) Projections onto the l axis of the two-dimensional data of Fig. 12(b) corresponding to the 40% fraction of the largest l triangles. Isolated points indicate the statistical accuracy of the bars on the histogram, and the theoretical curves correspond to different calculated models of the molecular structures involved (see text). n values refer to bending vibrational excitation.

by geometric than energetic parameters. The latter would presumably be very different for C_3 and NCO. The high excitation also provides a plausible interpretation of the relatively few needle shapes: as the system approaches the dissociation limit, the potential gradually flattens in slope as indicated schematically in Fig. 19; the motion is strongly anharmonic, and the system tends to concentrate in the extreme limits of its motion, away from the center. A possible and natural way to explain the observations would be to hypothesize that for the various species considered, in addition to being formed at high bending excitation, they also dissociate at a limiting angle θ, larger than 40°. The similarity of the data for all species of C_3 and NCO would appear, in this interpretation, to be accentuated by the insensitivity of the Coulomb-explosion process to the opening angle α_i $(=180°-\theta)$ in the range $\alpha_i \lesssim 140°$ (cf. Fig. 16).

Calculated l distributions are shown in Figs. 13(a) and 13(b). They were carried out for structures that yield a reasonable fit to the d/l data. The $n=7$ bending mode with the NCO parameters[9] and $n=2$ with the C_3 parameters[9] were chosen as the best-fit n values to the d/l distributions. Evidently, fixed separation structures yield quite reasonable fits to the data.

The data are summarized in Table I, and for the C_3 species, is all in accord with the internuclear separation of neutral C_3; $l_i=r_1+r_2=2.5(1)$ Å. For NCO, $l_i=2.0(1)$ Å was measured and is considerably smaller than the upper limit previously established.[9]

VII. CONCLUSION

It has been demonstrated that the technique described here is capable of furnishing valuable information on various aspects of molecular structure and vibrational excitation in accelerator ion sources. Specifically, it has been found that all the species that were studied are formed in states of high bending excitations, and somewhat indirectly, that these states appear to be close to the dissociation limit. Rather surprisingly, no major difference in the spectrum of bending amplitudes was found for the supposedly rigid NCO species and the floppy C_3. An hypothesis was proposed that the bending amplitude of both types of molecules are limited by breakup at angles somewhat larger than 40°.

No definite conclusions could be reached concerning the breathing-mode excitations except that the molecules considered are probably very stiff in this mode, as expected. Values for the intranuclear separations were established; the C_3 species were found to have the separations found in normal neutral C_3, i.e., $l_i=r_1+r_2=2.5(1)$ Å, and for NCO, the separation was determined to be rather small, $l_i=2.0(1)$ Å.

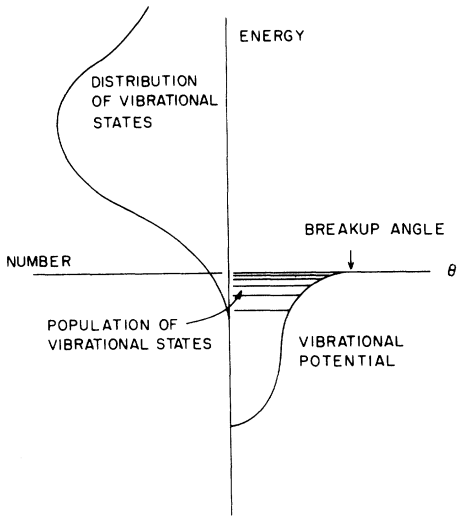

FIG. 19. Schematic diagram indicating a possible situation in which linear molecular ions would be formed in bending vibrational states close to the breakup point and assume bent configurations all the way up to the limit where they break up.

ACKNOWLEDGMENTS

The authors are grateful to Dr. Marshal Newton for helpful discussions, and to Professor Gerhard Herzberg for valuable suggestions and for his continued interest in this work.

[1]M. J. Gaillard, D. S. Gemmell, G. Goldring, I. Levine, W. J. Pietsch, J. C. Poizat, A. Y. Ratkowski, J. Remillieux, Z. Vager, and B. J. Zabransky, Phys. Rev. A 17, 1797 (1978).

[2]D. S. Gemmell, P. J. Cooney, and E. P. Kanter, Nucl. Instrum. Methods 170, 81 (1980).

[3]H. A. Oswald and R. V. Wheeler, Health Phys. 33, 650 (1977); Y. Eisen, *ibid.* 38, 497 (1980).

[4]P. Thieberger and H. E. Wegner, Nucl. Instrum. Methods 122, 205 (1974).

[5]Hiconex Model 852 Cs sputter ion source manufactured by the General Ionex Corp., 19 Gras Rd., Newburyport, Mass. 61950.

[6]D. D. Armstrong and H. E. Wegner, Rev. Sci. Instrum. 12, 40 (1971).

[7]P. Thieberger, Argonne National Laboratory Report No. ANL/FHY-79-3 (unpublished).

[8]D. S. Gemmell, T. Remillieux, J. C. Poizat, M. J. Gaillard, R. F. Holland, and Z. Vager, Phys. Rev. Lett. 34, 1420 (1975).

[9]G. Herzberg, *Molecular Spectra and Molecular Structure* (Van Nostrand, Princeton, N. J., 1966), Vol. 3, Table 64, p. 591.

[10]Z. Vager, in *Proceedings of the 38th Bat-Sheva Seminar, Bat-Sheva, Israel, 1980,* edited by Baruch Rosner (Annals of the Israel Physical Society, Jerusalem, 1981), Vol. 4.

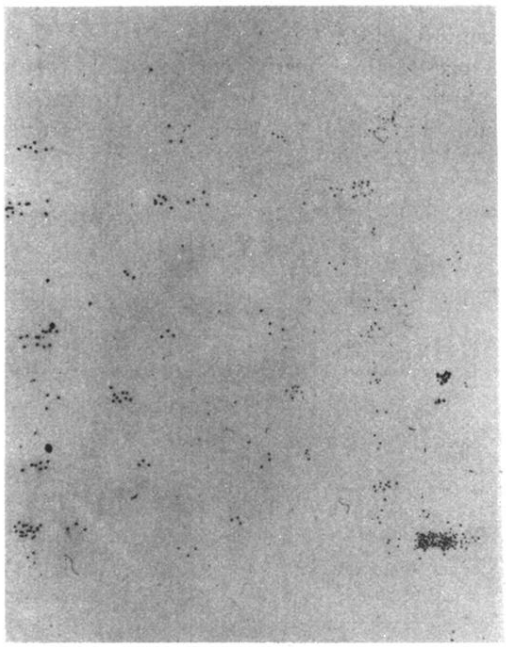

FIG. 3. Partially magnified electrochemically etched polycarbonate foil after exposure to stripped 4.67-MeV C_3^- ions.

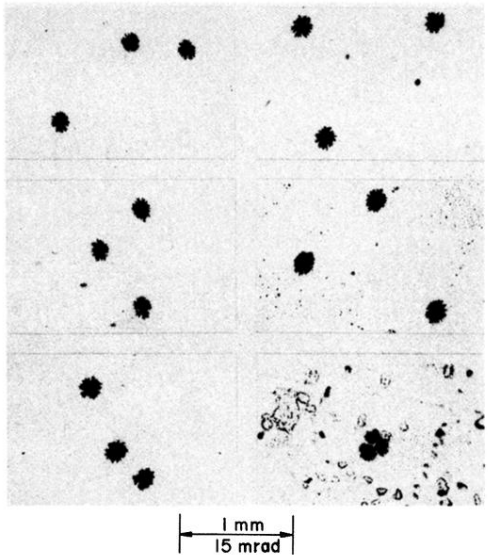

FIG. 4. Further magnification of selected C_3^- molecular explosion events at 4.67-MeV molecular-ion energy.

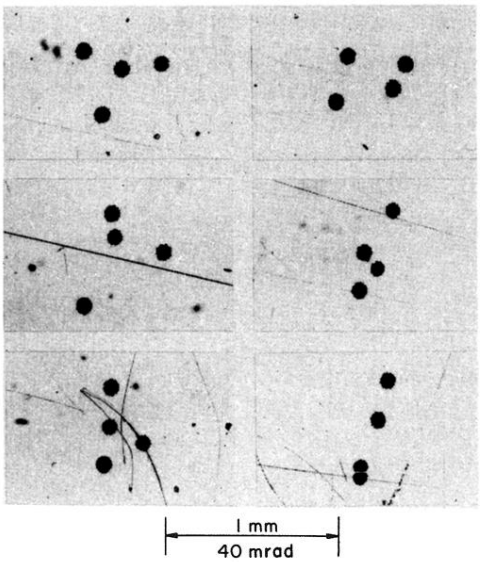

FIG. 5. Selected C_4^- molecular explosion events at 3.50-MeV molecular-ion energy.

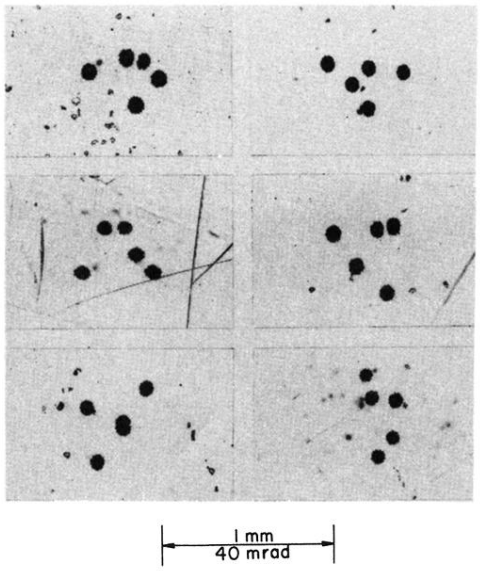

FIG. 6. Selected C_5^- molecular explosion events at 2.80-MeV molecular-ion energy.